



Research article

circUBAP2 ameliorates hypoxia-induced acute myocardial injury by competing with miR-148b-3p and mediating CDKN1B expression[☆]



FeiFei Li ^{a,1}, Li Xu ^{b,1}, JingMin Ou ^c, ZuWei Yang ^a, YuXin Dai ^c, MingKe Qiu ^c, Xin Hou ^{a,*}, DengFeng Zhu ^{d,*}

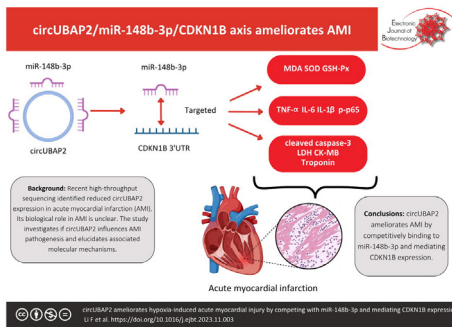
^a Department of Vascular Surgery and Intervention, Chongming Hospital Affiliated to Shanghai University of Medicine and Health Sciences, Shanghai City 201318, China

^b Department of Ultrasound, Chongming Hospital Affiliated to Shanghai University of Medicine and Health Sciences, Shanghai City 201318, China

^c Department of Interventional Vascular Surgery, Xinhua Hospital Affiliated to Shanghai Jiao Tong University School of Medicine, Shanghai City 200092, China

^d Department of General Surgery, Chongming Hospital Affiliated to Shanghai University of Medicine and Health Sciences, Shanghai City 201318, China

GRAPHICAL ABSTRACT



ARTICLE INFO

Article history:

Received 28 July 2023

Accepted 15 November 2023

Available online 13 December 2023

Keywords:

Acute myocardial infarction

CCK-8 assay

CDKN1B

circUBAP2

Flow cytometry

High-throughput sequencing

Inflammation

LDH release

Luciferase activity

ABSTRACT

Background: A recent high-throughput sequencing study revealed an anomalous underexpression of circular RNA UBAP2 (circUBAP2) in acute myocardial infarction (AMI), yet its biological function within this context remains elusive. This study aims to unravel whether circUBAP2 is instrumental in modulating the pathogenesis of AMI and to illuminate the underlying molecular mechanisms at play.

Results: circUBAP2 was abnormally low expressed in AMI. Inducing circUBAP2 ameliorated hypoxia-induced myocardial cell injury by enhancing cellular viability, and decreasing lactate dehydrogenase release, apoptosis, inflammation, and oxidative damage. circUBAP2 targeted miR-148b-3p, miR-148b-3p overexpression offset circUBAP2-induced cardioprotection. Cyclin-dependent kinase inhibitor 1B (CDKN1B) was mediated by miR-148b-3p, and CDKN1B upregulation suppressed the deleterious effect of circUBAP2 silencing on hypoxic AC16 cells. In addition, overexpression of circUBAP2 improved myocardial injury, decreased myocardial cell apoptosis, and alleviated inflammation and oxidative stress in AMI mice.

Conclusions: circUBAP2 ameliorates AMI by competitively binding to miR-148b-3p and mediating CDKN1B expression.

[☆] Audio abstract available in Supplementary material.

Peer review under responsibility of Pontificia Universidad Católica de Valparaíso

* Corresponding authors.

E-mail addresses: 1037982@qq.com (X. Hou), dengfeng246@hotmail.com (D. Zhu).

¹ These authors contributed equally to this study.

<https://doi.org/10.1016/j.ejbt.2023.11.003>

0717-3458/© 2023 The Authors. Published by Elsevier Inc. on behalf of Pontificia Universidad Católica de Valparaíso.

This is an open access article under the CC BY-NC-ND license (<http://creativecommons.org/licenses/by-nc-nd/4.0/>).

miR-148b-3p
RIP assay

How to cite: Li F, Xu L, Ou J, et al. circUBAP2 ameliorates hypoxia-induced acute myocardial injury by competing with miR-148b-3p and mediating CDKN1B expression. *Electron J Biotechnol* 2024;68. <https://doi.org/10.1016/j.ejbt.2023.11.003>.

© 2023 The Authors. Published by Elsevier Inc. on behalf of Pontificia Universidad Católica de Valparaíso. This is an open access article under the CC BY-NC-ND license (<http://creativecommons.org/licenses/by-nc-nd/4.0/>).

1. Introduction

Acute myocardial infarction (AMI) is ignited by persistent ischemia and hypoxia in the coronary artery and can be accompanied by heart failure, shock, or arrhythmia. It is well-proved that diabetes, hypercholesterolemia, smoking, hypertension, and mental patterns are thought to interact in complex ways with an individual's genetic predisposition to determine the long-term likelihood of CAD [1]. Right ventricular infarction, cardiogenic shock, acute mitral regurgitation, and free wall or ventricular septal rupture are complications of AMI [2,3]. To control and prevent disease progression, conventional treatment includes beta-adrenergic receptor blockers, antithrombotic drugs, nitrates, or calcium channel blockers [4].

CircRNAs are endogenous transcripts that are differentially expressed in species, developmental stages and pathology [5]. Molecular biology techniques make circRNAs regarded as noncoding RNAs that regulate gene function. Till now, the involvement of circRNAs in the pathophysiological process of AMI has been revealed [6,7]. circUBAP2 has been widely explored and generally classified as a tumor promoter in various cancers [8]. At present, only a report has suggested that circUBAP2 is correlated with microcirculation in patients with cardiogenic shock after extracorporeal membrane oxygenation (ECMO) [9]. However, in the course of AMI, its function has been narrowly mentioned and probed.

The mechanistic involvement of circRNAs in AMI is partially related to their regulation of circRNA-miRNA-mRNA network [10,11]. miR-148b-3p and its target CDKN1B were selected for studying circUBAP2-mediated AMI progression. miR-148b-3p has been once investigated in MI which is overexpressed during MI [12]. In addition to that, miR-148b-3p is responsible for modulating cardiomyocyte apoptosis under hypoxia/reoxygenation preconditioning [13]. As for CDKN1B (p27), a report has discovered the association between CDKN1B promoter DNA polymorphism and MI [14]. Moreover, it is established that CDKN1B haploinsufficiency prevents apoptosis in early MI by restoring autophagy fluxes [15].

Considering the significant involvement of circUBAP2, miR-148b-3p, and CDKN1B in cardiovascular diseases, this paper studied these three indexes in AMI by constructing a circRNA-miRNA-mRNA, hoping to develop and explore a novel therapeutic target based on genetics.

2. Materials and methods

2.1. Cell culture

Human cardiomyocytes (AC16) (BioVector NTCC, Beijing, China) were cultured in 10% FBS-DMEM (Gibco, NY, USA) supplementary with 1% penicillin/streptomycin (Invitrogen, USA). AC16 cells were cultured at 37°C in an anaerobic incubator containing 21% O₂ and 5% CO₂. For hypoxic treatment, cells were cultured for 24 h under 1% O₂ and 5% CO₂.

2.2. Cell transfection

siRNA or pcDNA 3.1 vectors targeting circUBAP2 and CDKN1B, miR-148b-3p mimic/inhibitor, and their negative controls (GenePharma, China) were transfected into AC16 cells using Lipofec-

tamine 3000 (Invitrogen) as requested by the manufacturer. RT-qPCR and Western blot assessed the transfection efficiency 48 h later.

2.3. Actinomycin D treatment

AC16 cells were cultured in six-well plates (5 × 10⁵ cells per well) for 24 h, exposed to 2 µg/ml actinomycin D (Sigma), and analyzed by RT-qPCR to assess RNA stability at a specified time point.

2.4. RNase R processing

RNA (10 µg) from AC16 cells was processed with RNase R (3 U/g, Epicenter) at 37°C for 30 min, followed by RT-qPCR analysis of circRNA and linear RNA.

2.5. RT-qPCR

Total RNA was extracted with Trizol reagent (Life Technologies), and RNA quality was measured using a NanoDrop 2000 spectrophotometer (Thermo Fisher Scientific). cDNA (circRNA/mRNA) was produced using PrimeScript RT Master Mix (Takara; RR036A) or PrimeScriptTMRT Reagent Kit (Takara; RR037A) for miRNA. RT-qPCR was conducted using the Roter Gene 3000 sequence detection system (Corbett Research, Australia) in combination with ChamQ SYBR qPCR Master Mix (Vazyme; Q311-02). Relative gene expression was calculated by 2^{-ΔΔCt} and normalized to GAPDH or U6. The primer sequence is shown in Table 1.

2.6. Western blot

To collect proteins, tissues and cells were processed with RIPA buffers (Thermo Fisher). Then, protein quantification was carried out with a BCA analysis kit (BioVision, CA, USA). The proteins were separated on 10% SDS gel, transferred to a PVDF membrane (Thermo Fisher), incubated in 5% milk, and then mixed with the primary antibodies overnight, as well as the HRP-coupled secondary antibody (BD Biosciences) for 1 h. Protein bands were evaluated using the SynGene system and GeneSnap software (SynGene, MD, USA). Primary antibodies are GAPDH (60004-1-Ig, Proteintech), cleaved caspase-3 (9664, Cell Signaling Technology), NF-κB (10745-1-AP, Proteintech), p-NF-κB (3031, Cell Signaling Technology), Troponin (MA5-12960, Invitrogen), CK-MB (ab404, Abcam).

2.7. CCK-8 experiment

AC16 cells were dispersed in 96-well plates, of which each well was supplemented with 10 µL CCK-8 solution (Beyotime, China) and let stand for another 4 h. Optical density (OD) at 450 nm was measured with a microplate reader. See [Equation 1].

$$\text{Cell viability} = \frac{(OD_{\text{experimentalgroup}} - OD_{\text{blankgroup}})}{(OD_{\text{controlgroup}} - OD_{\text{blankgroup}})} \times 100 \quad (1)$$

2.8. LDH detection

LDH release in AC16 cell culture was quantitatively assessed according to the Pierce LDH cytotoxicity Assay Kit protocol to

Table 1
Primers.

Genes	Primers (5'-3')
Human circUBAP2	Forward: 5'-GTCTTCACTGCCTCATCTGCT-3' Reverse: 5'-CCATGCCTTGGGTTGAGAAC-3'
Mouse circUBAP2	Forward: 5'-AGGTTCTCCGCTCAAAGCAT-3' Reverse: 5'- CCGGTCCTCATCTGTACCA-3'
MiR-148b-3p	Forward: 5'-GCGTCAGTGCATCACAGAA-3' Reverse: 5'- TGGTGTCTGGAGTTCG-3'
Human CDKN1B	Forward: 5'-GGCAAGTACGAGTGGCAAGA-3' Reverse: 5'-CGTGTCTCAGAGTTAGCCG-3'
U6	Forward: 5'-CTCGTTCGGCAGCACA-3' Reverse: 5'-AACGCTTCACGAATTTGCGT-3'
Human GAPDH	Forward: 5'-CACCACTCTCCACCTTTG-3' Reverse: 5'-CCACCACCTGTTGCTGTAG-3'
Mouse GAPDH	Forward: 5'-CATCAACGGGAAGCCATC-3' Reverse: 5'-CTCGTGGTTCACCCATC-3'

Note: circUBAP2, circular RNA ubiquitin-associated protein 2; MiR-148b-3p, MicroRNA-148b-3p; CDKN1B, cyclin-dependent kinase inhibitor 1B; GAPDH, Glyceraldehyde-3-phosphate dehydrogenase.

assess cytotoxicity (Thermo Scientific). In short, AC16 cells were centrifuged and the supernatant was removed. The standard hole was added with 5 μ L water and 20 μ L pyruvate solution. The sample hole was added with 20 μ L sample and 5 μ L water. The control hole was added with 20 μ L sample. Each hole was added with 25 μ L buffer. Then, 5 μ L coenzyme I was added to the sample hole and incubated at 37°C for 15 min. Next, 25 μ L color developer was supplemented and incubated for another 15 min. Also, 250 μ L alkaline reagent was added to each well and let stand at room temperature for 5 min. Absorbance (A) values of each hole were measured at 450 nm. See [Equation 2]

$$\text{LDH activity} \left(\frac{\text{U}}{\text{gprot}} \right) = \frac{\Delta 450 - b}{a} \times f \div \text{Cpr} \times 1000 \quad (2)$$

2.9. Flow cytometry

Annexin V-FITC apoptosis detection kit (Vazyme) was applied in this assay. Simply, AC16 cells after treatment with cold PBS (Sangon, Shanghai, China) were resuspended in a binding buffer, and the suspension was prepared into a mixture with 5 μ L Annexin V-FITC and 5 μ L PI and placed darkly for 15 min before detection on a flow cytometer (Beckman Coulter, GA, USA).

2.10. ELISA

TNF- α , IL-1 β , and IL-6 in myocardial tissue and AC16 cells were determined using ELISA kits (Solarbio, Beijing, China). Cell supernatant or tissue homogenate supernatant was collected. Required reagents and standards were prepared. Standard holes, 0 holes, and sample holes were set. The ELISA plate was immersed, added with the standard and sample, and incubated at 37°C for 90 min. After washing four times, biotin was added to detect antibodies and incubated for 60 min. After washing again four times, enzyme conjugate was incubated for 30 min. Next, after washing again five times, TMB color-developing substrate was incubated for 15 min at 37°C in darkness, and OD value at 450 nm was read on a microplate reader.

2.11. Oxidative damage assessment

MDA, SOD, and GSH-PX in tissues and cells were measured using commercial kits (Jiancheng Bioengineering Institute, Nanjing, China). The standard and corresponding reagents were added to the 96 plates in accordance with the manufacturer's method, then transferred to a centrifugal tube, mixed with a vortex mixer,

and bathed in a boiling water bath for 40 min. The supernatant was removed after centrifugation. MDA, SOD, and GSH-PX were measured by reading optical values at 532 nm, 450 nm, and 412 nm, respectively.

2.12. Analysis of luciferase activity

The wild-type (WT) circUBAP2 and CDKN1B 3'-UTR fragments containing predicted miR-148b-3p binding sites were amplified and inserted into pmirGLO (Promega) to establish circUBAP2-WT and CDKN1B-WT. GeneArt™ site-directed mutagenesis PLUS system (A14604; Thermo Fisher Scientific) mutated the putative binding site of miR-148b-3p in circUBAP2 and CDKN1B 3'-UTR. The mutant (Mut) circUBAP2 and CDKN1B 3'-UTR were inserted into the pmirGLO vector to construct circUBAP2-mut and CDKN1B-mut. The reporter vector and miR-148b-3p mimic or mimic NC were co-transfected into AC16 cells using Lipofectamine 3000 reagent. Luciferase activity measurements were conducted in a dual luciferase reporting system (Promega) after 48 h.

2.13. RIP experiment

RIP testing was performed using a RIP kit (Millipore, MA, USA). In short, the AC16 cells were cleaved using the RIP cleavage buffer. Next, RIP buffers containing magnetic beads conjugated with human anti-Ago2 were added to the cell extracts. Protease K was then applied to digest the protein and isolate the immunoprecipitated RNA for RT-qPCR.

2.14. Establishment of AMI mouse model

Forty male C57BL/6 mice (Laboratory Animal Center of Chongming Hospital Affiliated to Shanghai University of Medicine and Health Sciences) were placed in a standard laboratory environment with a light-dark period of 12 h, 22–24°C, and 50–60% humidity. Food and water were supplied enough during the experiment. This experimental protocol was approved by the Animal Care and Use Committee of Chongming Hospital Affiliated to Shanghai University of Medicine and Health Sciences. Thirty mice underwent permanent left anterior descent (LAD) ligation to construct an AMI model: The mice were anesthetized with pentobarbital sodium (30 mg/kg) and connected to a ventilator (DW-3000B; Sunstar, Beijing, China) with 100 breaths/min and 100 ml stroke volume. Then, thoracotomy was implemented on the left side and the LAD was ligated with an 8-0 suture. Throughout the experiment, the mice had an 80 percent survival rate. No LAD ligation was conducted in sham group. A lentiviral overexpression vector targeting circUBAP2 (oe-circUBAP2, Beyotime) was injected into mice via the tail vein three days before surgery (1×10^7 TU). After 12 h of LAD ligation, CO₂ inhalation was required to euthanize mice, from which blood and myocardial tissue were harvested and stored at –80°C.

2.15. Hematoxylin and eosin (HE) staining

Myocardial tissue was fixed with 4% paraformaldehyde. After dehydration by alcohol gradient, the tissue was embedded in paraffin wax and cut into 4 μ m slices. After HE staining (Beyotime), the sections were sealed, examined, and photographed under a microscope.

2.16. TUNEL staining

Apoptotic cells in myocardial tissue were tested by One-Step TUNEL Apoptosis Assay kit (Roche). In short, paraffin sections after hydration were incubated with protease K for 20 min and with dUTP solution and TdT enzymes at 37°C for 1 h. DNase I incubation

(25°C) for 10 min before fluorescence labeling was considered a positive control, while dUTP incubation was a negative one. Next, the sections were processed with DAPI (Sigma-Aldrich; Merck KGaA), which was followed by treatments with gradient ethanol for dehydration, xylene for alum, and neutral balsam for loading. The images were observed using a microscope (Carl Zeiss, LSM700).

2.17. IHC staining

After dewaxing and hydration, the sections were sealed with 3% H₂O₂, covered with 10% normal goat serum (No. 16210072; Gibco; Thermo Fisher Scientific), and incubated with primary antibodies including Troponin (MA5-12960, Invitrogen) and CK-MB (ab404, Abcam) overnight. Then, HRP-coupled goat anti-rabbit secondary antibody (1:400; A32731; Invitrogen) was incubated together, and then, DAB was added for color development. Image capture was done with a microscope.

2.18. Data analysis

Data were analyzed using GraphPad Prism 9.0 software and expressed as mean ± standard deviation (SD). The unpaired student t-test was used to assess the difference between the two groups, while one-way ANOVA and Tukey post hoc tests were to assess that across groups. $P < 0.05$ suggested a significant difference. All experiments were biologically replicated at least three times.

3. Results

3.1. circUBAP2 is abnormally low expressed in AMI

AC16 cell damage was induced by hypoxia to simulate MI *in vitro*. The AMI mouse model was established by LAD ligation. We first evaluated the circUBAP2 expression pattern in AMI. Hypoxia reduced circUBAP2 expression in AC16 cells (Fig. 1A), and circUBAP2 in AMI mice was lower than that in Sham mice (Fig. 1B). We then examined the circUBAP2 (circbase ID: hsa_circ_0001848) gene information through the bioinformatics website and found hsa_circ_0001848 location (chr9: 33956076–33973235 strand: -) with the length of the splicing sequence of 346 bp (Fig. 1C). We then evaluated the circUBAP2 ring structure: Actinomycin D was not able to affect the stability of circUBAP2 RNA (Fig. 1D), and RNase R reduced GAPDH RNA expression but did not affect circUBAP2 RNA expression (Fig. 1E).

3.2. Inducing circUBAP2 ameliorates hypoxia-induced myocardial injury

pcDNA 3.1 plasmid targeting circUBAP2 was transfected into hypoxia-induced AC16 cells. As a result, pcDNA 3.1-circUBAP2 forced circUBAP2 levels in AC16 cells (Fig. 2A). In terms of function, CCK-8 test revealed that hypoxia reduced cell viability in AC16 cells, but inducing circUBAP2 partially restored cell viability in AC16 cells (Fig. 2B). Myocardial cells are usually accompanied by LDH release when AMI injury occurs. We then assessed the level of LDH in the cells. Hypoxia increased LDH levels in AC16 cells, but inducing circUBAP2 significantly reduced LDH release (Fig. 2C). Subsequently, when exploring apoptosis rate using flow cytometry, hypoxia was found to elevate AC16 cell apoptosis, but this effect was attenuated by inducing circUBAP2 (Fig. 2D). The cellular ability to release inflammatory factors was then detected by ELISA, revealing that hypoxia increased TNF- α , IL-1 β , and IL-6 levels in the cell supernatant, but inducing circUBAP2 dampened levels of these three inflammatory agents (Fig. 2E). Also, hypoxia

elevated MDA levels and inactivated SOD and GSH-Px in AC16 cells, while inducing circUBAP2 prevented these changes (Fig. 2F). Subsequently, the changes of AC16 cell damage-related proteins were further evaluated by Western blot, presenting that hypoxia increased cleaved caspase-3, p-p65, Troponin, and CK-MB protein expression in AC16 cells, while inducing circUBAP2 lowered levels of these proteins (Fig. 2G).

3.3. circUBAP2 targets miR-148b-3p

CircRNAs usually perform biological functions by competitively adsorbing miRNAs and mediating downstream mRNA expression. Therefore, we next explore potential downstream miRNAs for circUBAP2. Potential binding sites for circUBAP2 and miR-148b-3p were found as predicted by starbase, a bioinformatics website (Fig. 3A). Subsequently, we examined whether they were targeted binding in AC16 cells. When analyzing the targeting relationship in dual luciferase reporter experiment, WT-circUBAP2 in combination with miR-148b-3p mimic caused the repression of luciferase activity, but MUT-circUBAP2 scheme did not reduce luciferase activity (Fig. 3B). RIP evaluation results manifested that Ago2 magnetic beads were capable of enriching circUBAP2 and miR-148b-3p (Fig. 3C). miR-148b-3p was highly expressed in hypoxia-incubated AC16 cells and in myocardial tissue of AMI mice (Fig. 3D,E). Interestingly, overexpression or underexpression of circUBAP2 decreased and increased miR-148b-3p expression in AC16 cells, respectively (Fig. 3F).

3.4. circUBAP2 protects hypoxic cardiomyocytes by regulating miR-148b-3p

Subsequently, whether miR-148b-3p participated in the circUBAP2 regulation process of myocardial cell damage was explored through functional rescue experiments. pcDNA 3.1-circUBAP2 and miR-148b-3p mimic were co-processed into AC16 cells treated with hypoxia. The inhibition of pcDNA 3.1-circUBAP2 on miR-148b-3p in AC16 cells was reversed by miR-148b-3p mimic (Fig. 4A). Followed by that, several function assays found that although circUBAP2 overexpression protected cardiomyocytes against hypoxic damages regarding cell viability, LDH release, apoptosis, inflammatory cytokines, oxidative damage markers, and AC16 cell damage-related proteins, miR-148b-3p elevation blocked these protective procedures (Fig. 4B–G).

3.5. CDKN1B is mediated by miR-148b-3p

Potential binding sites for miR-148b-3p and CDKN1B were predicted through bioinformatics websites (Fig. 5A). Subsequently, we evaluated their targeting relationships. Dual luciferase reporting experiments showed that co-transfection of WT-CDKN1B and miR-148b-3p mimic reduced luciferase activity (Fig. 5B) and RIP experiments showed highly enriched CDKN1B and miR-148b-3p in Ago2 magnetic beads (Fig. 5C). We then examined CDKN1B expression pattern in AMI. CDKN1B in AMI mice was decreased (Fig. 5D), and its expression was decreased after hypoxia treatment, but knocking down miR-148b-3p increased CDKN1B expression, while inducing miR-148b-3p further dampened CDKN1B expression (Fig. 5E).

3.6. circUBAP2 ameliorates hypoxia-induced myocardial injury by miR-148b-3p/CDKN1B axis

Subsequently, si-circUBAP2 and pcDNA 3.1-CDKN1B were co-transfected into AC16 cells treated with hypoxia. si-circUBAP2 increased miR-148b-3p and decreased CDKN1B levels. pcDNA 3.1-CDKN1B increased CDKN1B but did not affect miR-148b-3p

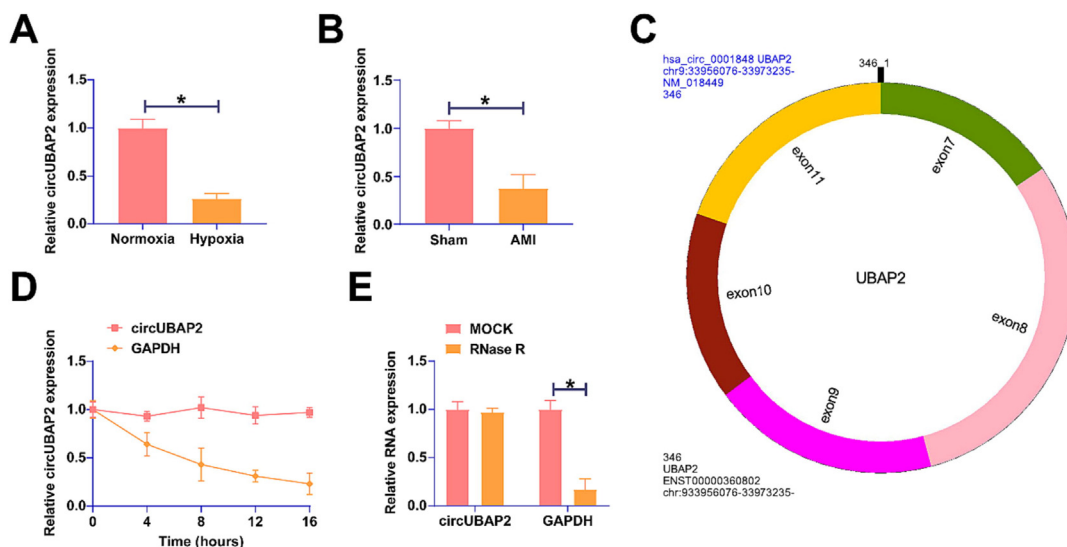


Fig. 1. Circubap2 is abnormally low expressed in ami. (A) RT-qPCR measurement of circUBAP2 level in hypoxia-induced AC16 cells. (B) RT-qPCR measurement of circUBAP2 in myocardial tissue of AMI mice and Sham group. (C) circUBAP2 gene information; (D) Actinomycin D test evaluation of the circular structure of circUBAP2. (E) RNase R assessment of circUBAP2 circular structure experimentally. Data were expressed as mean \pm SD (A, C, D, E, n = 3; B, n = 6). * $P < 0.05$.

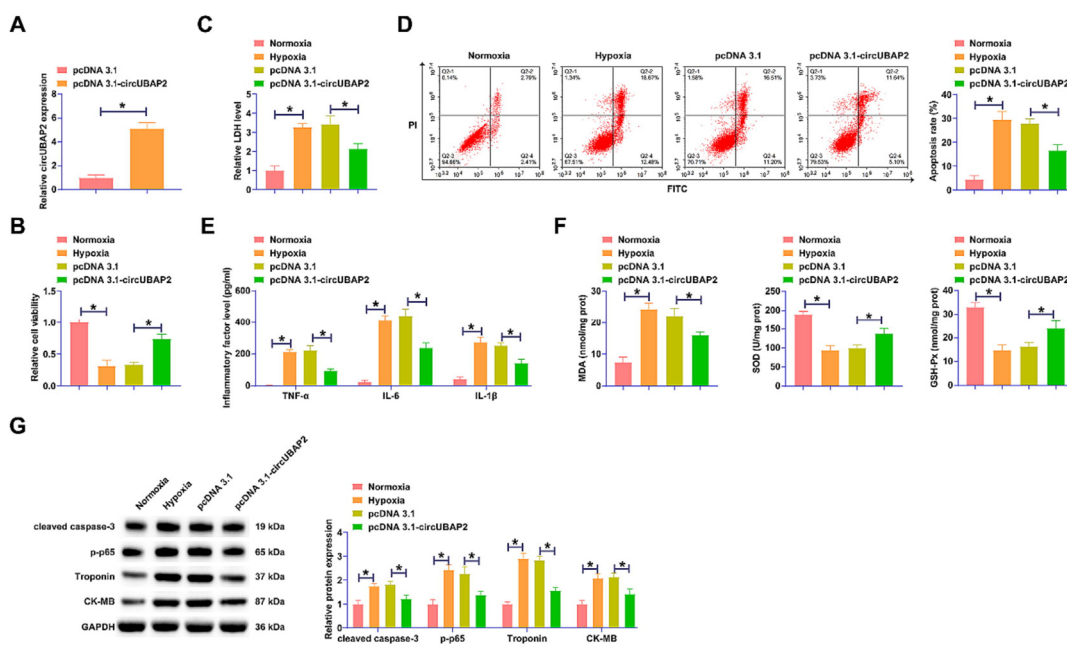


Fig. 2. Inducing circUBAP2 ameliorates hypoxia-induced myocardial cell injury. pcDNA 3.1 overexpressed plasmid targeting circUBAP2 was transfected into hypoxia-induced AC16 cells. (A) RT-qPCR measurement of circUBAP2 in AC16 cells. (B) CCK-8 assay analysis of cell viability. (C) Commercial kit to detect LDH release from cells. (D) Flow cytometry detection of cell apoptosis rate. (E) ELISA evaluation of inflammatory cytokines TNF- α , IL-1 β and IL-6 in the supernatant. (F) Commercial kits to detect MDA, SOD and GSH-Px in cells. (G) Western blot measurements of cleaved caspase-3, p-p65, Troponin, and CK-MB. Data were expressed as mean \pm SD (n = 3). * $P < 0.05$.

expression levels (Fig. 6A). Moreover, decreasing circUBAP2 reduced cell viability in AC16 cells, promoted LDH release, increased apoptosis rate, elevated levels of cellular inflammatory cytokines, increased MDA levels and reduced SOD and GSH-Px levels, and promoted cleaved caspase-3, p-p65, Troponin, and CK-MB, while inducing CDKN1B prevented changes mediated by circUBAP2 knockdown (Fig. 6B–G).

3.7. circUBAP2 improved myocardial infarction in AMI mice

Subsequently, a lentivirus overexpression vector targeting circUBAP2 was injected into AMI mice. injection of the

oe-circUBAP2 lentivirus vector successfully forced circUBAP2 and CDKN1B and decreased miR-148b-3p expression in AMI mice (Fig. 7A). HE staining showed cardiomyocyte atrophy and necrosis in AMI mice with disordered cell arrangement, which was improved by oe-circUBAP2 (Fig. 7B). TUNEL staining showed that the TUNEL positive rate was higher in the myocardium of AMI mice than in Sham mice, and oe-circUBAP2 reduced the proportion of TUNEL positive cells in AMI mice (Fig. 7C). ELISA results showed that TNF- α , IL-1 β and IL-6 were increased in myocardium of AMI mice, but oe-circUBAP2 blocked these changes (Fig. 7D). Inducing circUBAP2 significantly reduced oxidative stress in myocardium of AMI mice (Fig. 7E). IHC staining determined that Troponin and

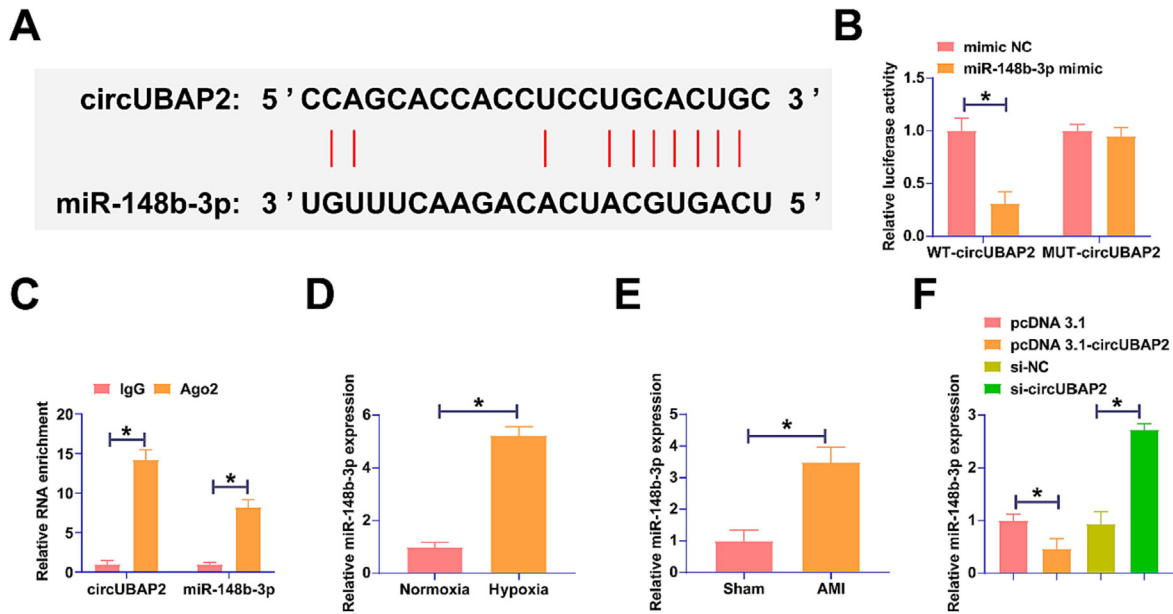


Fig. 3. Circubap2 targets mir-148b-3p. (A) Bioinformatics website starbase predicted potential binding sites for circUBAP2 and miR-148b-3p. (B-C) Dual luciferase reporter experiment and RIP assessment of the targeting relationship between circUBAP2 and miR-148b-3p. (D) RT-qPCR measurement of miR-148b-3p in AC16 cells induced by hypoxia. (E) RT-qPCR measurement of miR-148b-3p in myocardial tissue of AMI mice and Sham group (F) RT-qPCR measurement of the effect of circUBAP2 overexpression or knockdown on miR-148b-3p in AC16 cells. Data were expressed as mean ± SD (n = 3). * P < 0.05.

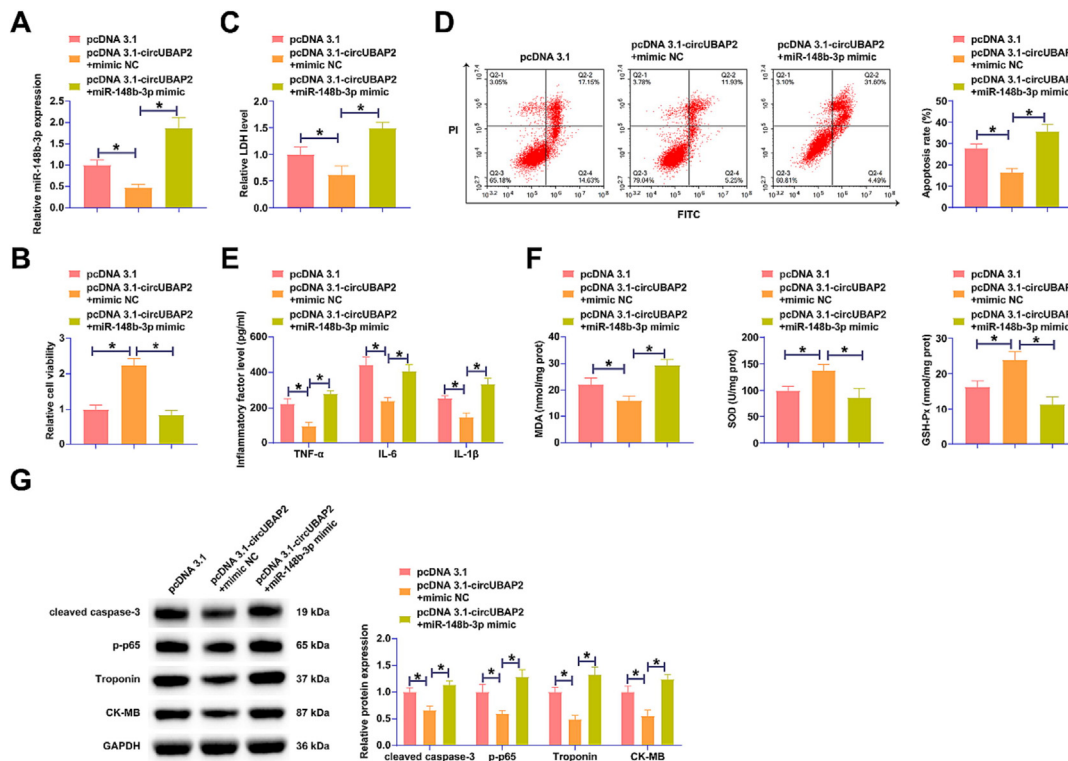


Fig. 4. Circubap2 protects hypoxic cardiomyocytes by regulating mir-148b-3p. pcDNA 3.1-circUBAP2 and miR-148b-3p mimic were co-transfected into AC16 cells treated with hypoxia. (A) RT-qPCR measurement of miR-148b-3p in AC16 cells. (B) CCK-8 assay analysis of cell viability. (C) Commercial kit to detect LDH release from cells. (D) Flow cytometry detection of cell apoptosis rate. (E) ELISA evaluation of inflammatory cytokines TNF-α, IL-6 and IL-1β in the supernatant. (F) Commercial kits to detect MDA, SOD and GSH-Px in cells. (G) Western blot measurements of cleaved caspase-3, p-p65, Troponin, and CK-MB. Data were expressed as mean ± SD (n = 3). * P < 0.05.

CK-MB were significantly increased in myocardium of AMI mice, but elevating circUBAP2 significantly decreased the expressions of these two proteins (Fig. 7F). In addition, Western blot confirmed

that inducing circUBAP2 effectively reduced cleaved caspase-3 and p-p65 levels in AMI mice (Fig. 7G).

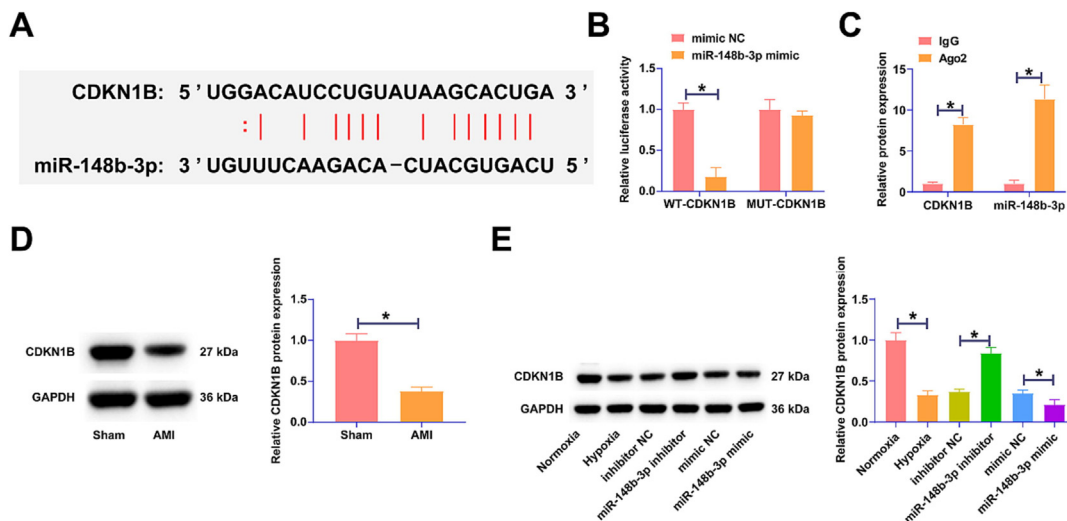


Fig. 5. CDKN1B is mediated by miR-148b-3p. (A) Bioinformatics website starbase predicted the potential binding sites of CDKN1B and miR-148b-3p. (B-C) Dual luciferase reporter experiment and RIP assessment of the targeting relationship between CDKN1B and miR-148b-3p. (D) Western blot measurements of CDKN1B in myocardial tissue of AMI mice. (E) Western blot measurements of CDKN1B in AC16 cells induced by hypoxia. Data were expressed as mean ± SD (n = 3). * P < 0.05.

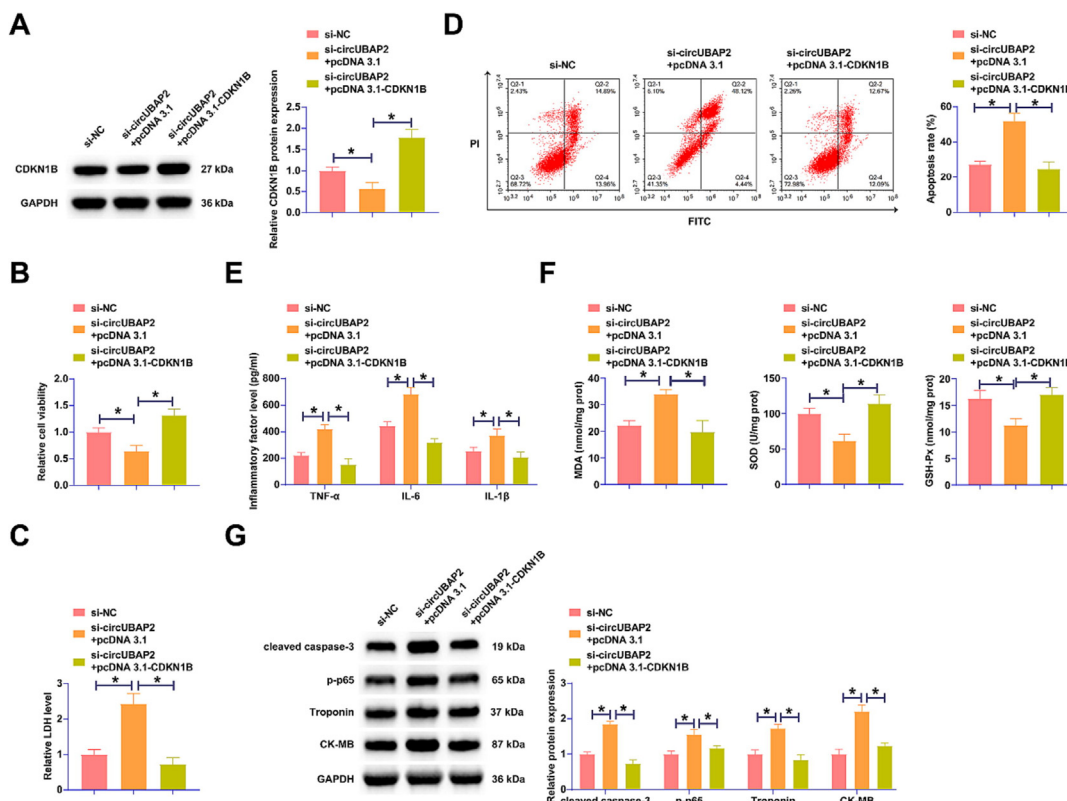


Fig. 6. Circubap2 ameliorates hypoxia-induced myocardial injury by miR-148b-3p/cdkn1b axis. si-circUBAP2 and pcDNA 3.1-CDKN1B were co-transfected into AC16 cells treated with hypoxia. (A) RT-qPCR and western blot measurements of circUBAP2/miR-148b-3p/CDKN1B in AC16 cells. (B) CCK-8 assay analysis of cell viability. (C) Commercial kit to detect LDH release from cells. (D) Flow cytometry detection of cell apoptosis rate. (E) ELISA evaluation of inflammatory cytokines TNF-α, IL-1β and IL-6 in the supernatant. (F) Commercial kits to detect MDA, SOD and GSH-Px in cells. (G) Western blot measurements of cleaved caspase-3, p-p65, Troponin, and CK-MB. Data were expressed as mean ± SD (n = 3). * P < 0.05.

4. Discussion

AMI, characterized by sudden cardiac death, is life-threatening to human society. To understand the mechanistic action of circRNAs in this disease, we performed this study analysis of circUBAP2, in combination with its complex interplay with miR-148b-

3p and CDKN1B. As a result, circUBAP2 could be considered a feasible protector in AMI by upregulating miR-148b-3p through competitive absorption of miR-148b-3p.

In recent years, research has begun to elucidate the intricate biological roles played by circRNAs in AMI. One such example is the circRNA CDYL, which instigates myocardial regeneration

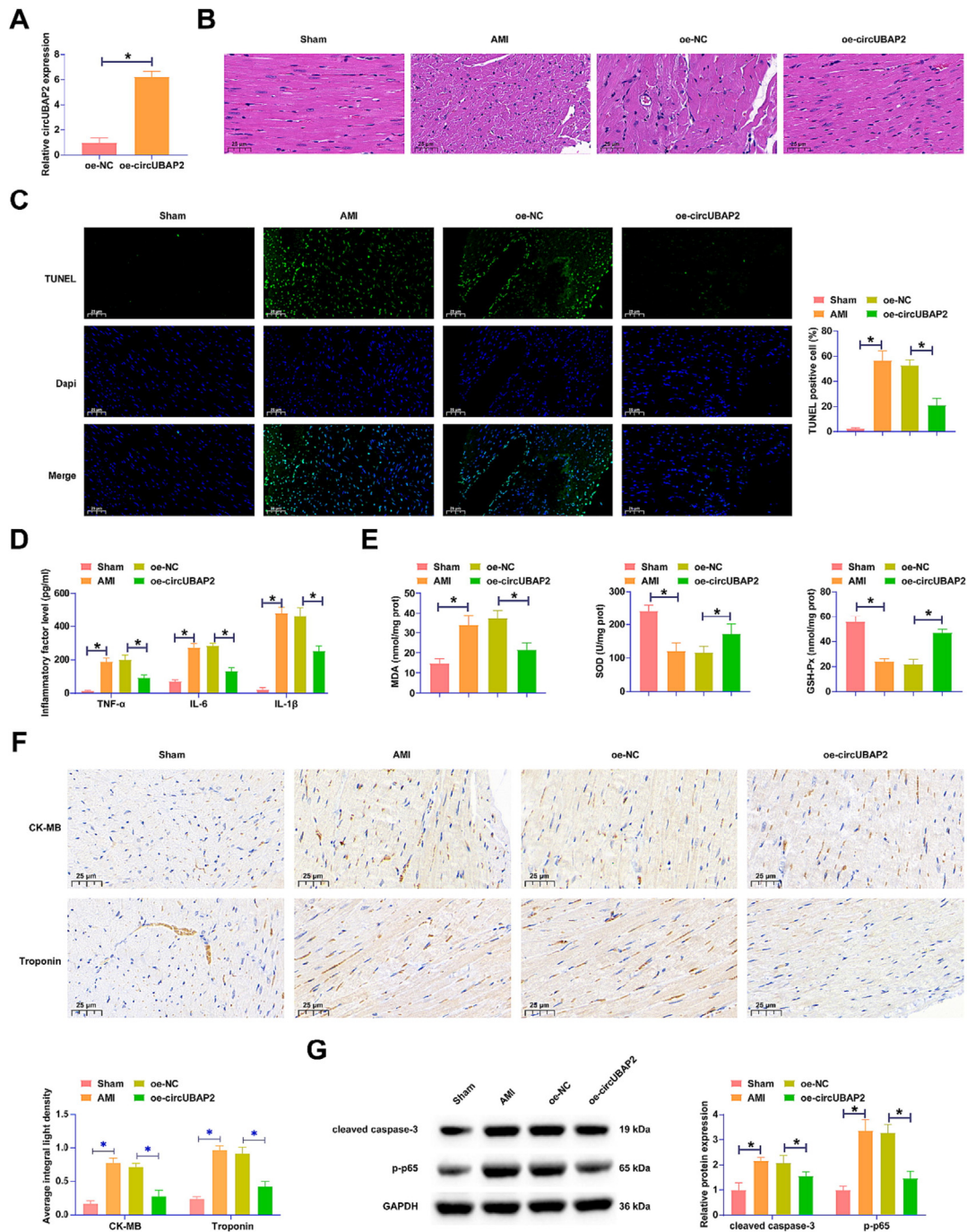


Fig. 7. Circubap2 improves myocardial infarction in ami mice. (A) RT-qPCR and western blot measurements of circUBAP2/miR-148b-3p/CDKN1B in AMI mice. (B) Representative images of HE staining of mouse myocardial tissue. (C) Representative images of TUNEL staining of myocardial tissue. (D) ELISA evaluation of TNF- α , IL-1 β and IL-6 in mouse myocardial tissue. (E) Commercial kits to detect MDA, SOD and GSH-Px in myocardial tissue. (F) IHC staining of Troponin and CK-MB in mouse myocardial tissue. (G) Western blot measurements of cleaved caspase-3 and p-p65. Data were expressed as mean \pm SD (n = 6). * P < 0.05.

post-infarction through its functioning as a ceRNA [16]. Overexpression of circRNA SNRK was observed to inhibit miR-103-3p in rats with myocardial infarction. This, in turn, regulates the GSK3 β /beta-catenin signaling pathway, leading to reduced apoptosis and promoting cardiac repair [17]. A comprehensive exploration of the circRNA-miRNA-mRNA network amidst the pathological process of AMI is instrumental in advancing targeted pharmacotherapeutic innovations. Current research has predominantly been centered on the biological functions of circUBAP2 in cancer. CircUBAP2 is renowned for its oncogenic role where it is implicated in the modulation of cancer cell proliferation, invasion, migration,

and epithelial-mesenchymal transition [18,19]. Interestingly, a previous high-throughput sequencing highlighted an anomalously low expression of circUBAP2 in AMI [20]. This study unveiled that circUBAP2 overexpression significantly ameliorated myocardial cell apoptosis, inflammation, and oxidative stress during the onset of AMI. These improvements were tightly associated with the inhibition of the p65 pathway activation. Consistent with our findings, an earlier study showed that circUBAP2 expression was significantly reduced in patients with cardiogenic shock and that circUBAP2 promoted macrophage M2 polarization and inhibited the activation of PI3K/Akt and mTOR pathways [9]. The inhibitory

effect of circUBAP2 on the p65 pathway may be instrumental in precluding macrophage migration and M1 polarization, a hypothesis warranting rigorous scrutiny in subsequent studies.

Current literature only sparingly addresses the role of circUBAP2 in the context of AMI, highlighting a significant knowledge gap and underscoring the necessity for extensive investigations to elucidate its underlying mechanisms. We were particularly intrigued by miR-148b-3p, identified as a downstream target of circUBAP2, echoing the “miRNA decoy” theory. This miRNA exhibits a persistent elevation in both hypoxic AC16 cells and AMI-afflicted mice, with its upregulation seemingly attenuating the protective effects conferred by circUBAP2 under hypoxic conditions [12]. The pathological elevation of miR-148b-3p, corroborated by a study involving hypoxic H9c2 cells, exacerbates apoptosis and inflammation while concurrently undermining cellular viability [14]. Sun et al. [13] echoed these findings, revealing an accentuated expression of miR-148b-3p following hypoxia/reoxygenation treatment, which correlates with compromised cellular viability, increased LDH release, and heightened apoptosis. Likewise, an analogous trend is observed in H9c2 cells, wherein miR-148b amplifies apoptotic incidences post-hypoxia/reoxygenation, undermining cell viability and SOD activity while promoting LDH and MDA levels [21]. It is becoming increasingly clear that miR-148b-3p is a detrimental player in the context of AMI, with a plethora of empirical data attesting to its malicious effects on cellular integrity and function. One of the salient revelations from our research was the identification of CDKN1B as a direct target of miR-148b-3p. We discerned an attenuated expression of CDKN1B in AMI specimens, and the induction of CDKN1B alleviated the deleterious impacts instigated by circUBAP2 silencing under a hypoxic milieu. The nuanced role of CDKN1B in cardiovascular pathology is further substantiated by investigations in diabetic cardiomyopathy, where its silencing is associated with exacerbated myocardial histology and inhibited cardiomyocyte autophagy [22]. Conversely, CDKN1B haploinsufficiency ameliorates cardiac function post-MI, mediated by the secretion of growth factors that foster angiogenesis and myocardial preservation [15]. Extending our gaze beyond the cardiac context, insights from cerebral ischemic stroke research indicate that decitabine augments CDKN1B expression by counteracting DNA methylation, resulting in reduced neuronal death and infarct volume [23]. This underscores the multidimensional influence of CDKN1B, extending its relevance beyond the confines of cardiac pathology. In essence, these collective insights underscore the imperative to deepen our understanding of the complex interplay between circUBAP2, miR-148b-3p, and CDKN1B. An in-depth elucidation of their synergistic and antagonistic interactions could pave the path for novel therapeutic interventions, not only in the realm of AMI but also potentially extending to a spectrum of cardiovascular and neurovascular disorders. Unraveling these molecular intricacies will be paramount in devising targeted, efficacious strategies to mitigate, and potentially reverse, the devastating impacts of these pathologies.

In summary, circUBAP2 ameliorates hypoxia-induced acute myocardial injury by competitively binding to miR-148b-3p and mediating CDKN1B expression. This analysis report supplies data support for widening molecules-based therapy for AMI. However, only laboratory experiments were conducted and the collected data were limited to cells and animals. Therefore, for generalization, clinical verification is materially required. Moreover, other mechanistic molecules of circUBAP2 are waiting for further investigations.

Ethical approval

The present study was approved by the Animal experiments which were approved by Chongming Hospital Affiliated to Shanghai University of Medicine and Health Sciences and all procedures

complied with the National Institutes of Health Guide for the Use of Laboratory Animals.

Author contributions

- Study conception and design: F Li; L Xu; X Hou; D Zhu.
- Data collection: J Ou; Z Yang.
- Analysis and interpretation of results: Y Dai; M Qiu.
- Draft manuscript preparation: F Li; L Xu.
- Revision of the results and approval of the final version of the manuscript: X Hou; D Zhu.

Financial support

This research did not receive any specific grant from funding agencies in the public, commercial, or not-for-profit sectors.

Conflict of interest

The authors have no conflicts of interest to declare.

Supplementary material

<https://doi.org/10.1016/j.ejbt.2023.11.003>.

Data availability

The datasets used and/or analyzed during the present study are available from the corresponding author on reasonable request.

References

- [1] Colombo A, Proietti R, Čulić V, et al. Triggers of acute myocardial infarction: A neglected piece of the puzzle. *J Cardiovasc Med* 2014;15(1):1–7. <https://doi.org/10.2459/JCM.0b013e3283641351>. PMID: 24500234.
- [2] Bajaj A, Sethi A, Rathor P, et al. Acute complications of myocardial infarction in the current era: Diagnosis and management. *J Investig Med* 2015;63(7):844–55. <https://doi.org/10.1097/JIM.0000000000000232>. PMID: 26295381.
- [3] Damluji AA, van Diepen S, Katz JN, et al. Mechanical complications of acute myocardial infarction: A scientific statement from the American Heart Association. *Circulation* 2021;144(2):e16–35. <https://doi.org/10.1161/CIR.0000000000000985>.
- [4] Saito Y, Oyama K, Tsujita K, et al. Treatment strategies of acute myocardial infarction: Updates on revascularization, pharmacological therapy, and beyond. *J Cardiol* 2023;81(2):168–78. <https://doi.org/10.1016/j.jicc.2022.07.003>. PMID: 35882613.
- [5] Huang A, Zheng H, Wu Z, et al. Circular RNA-protein interactions: Functions, mechanisms, and identification. *Theranostics* 2020;10(8):3503–17. <https://doi.org/10.7150/thno.42174>. PMID: 32206104.
- [6] Zhang S, Wang W, Wu X, et al. Regulatory roles of circular RNAs in coronary artery disease. *Mol Ther Nucleic Acids* 2020;21:172–9. <https://doi.org/10.1016/j.omtn.2020.05.024>. PMID: 32585625.
- [7] Altesha MA, Ni T, Khan A, et al. Circular RNA in cardiovascular disease. *J Cell Physiol* 2019;234(5):5588–600. <https://doi.org/10.1002/jcp.27384>. PMID: 30341894.
- [8] Sun J, Yin A, Zhang W, et al. CircUBAP2 inhibits proliferation and metastasis of clear cell renal cell carcinoma via targeting miR-148a-3p/FOXK2 pathway. *Cell Transplant* 2020;29:.. <https://doi.org/10.1177/0963689720925751>. PMID: 32425115963689720925751.
- [9] Li J, Yu Z, Zeng J, et al. Circular RNA UBAP2 (hsa_circ_0007367) correlates with microcirculatory perfusion and predicts outcomes of cardiogenic shock patients undergoing extracorporeal membrane oxygenation support. *Shock* 2022;57(6):200–10. <https://doi.org/10.1097/SHK.0000000000001937>. PMID: 35759302.
- [10] Wu J, Li C, Lei Z, et al. Comprehensive analysis of circRNA-miRNA-mRNA regulatory network and novel potential biomarkers in acute myocardial infarction. *Front Cardiovasc Med* 2022;9:.. <https://doi.org/10.3389/fcvm.2022.850991>. PMID: 35872921850991.
- [11] Zhou J, He S, Wang B, et al. Construction and bioinformatics analysis of circRNA-miRNA-mRNA network in acute myocardial infarction. *Front Genet* 2022;13:.. <https://doi.org/10.3389/fgene.2022.854993>. PMID: 35422846854993.
- [12] Wang S, Cheng Z, Chen X, et al. Long noncoding RNA SNHG4 attenuates the injury of myocardial infarction via regulating miR-148b-3p/DUSP1 axis.

- Cardiovasc Ther 2022;2022:1652315. <https://doi.org/10.1155/2022/1652315>. PMID: 36545243.
- [13] Sun M, Zhai M, Zhang N, et al. MicroRNA-148b-3p is involved in regulating hypoxia/reoxygenation-induced injury of cardiomyocytes in vitro through modulating SIRT7/p53 signaling. *Chem Biol Interact* 2018;296:211–9. <https://doi.org/10.1016/j.cbi.2018.10.003>. PMID: 30308185.
- [14] Rodríguez I, Coto E, Reguero JR, et al. Role of the CDKN1A/p21, CDKN1C/p57, and CDKN2A/p16 genes in the risk of atherosclerosis and myocardial infarction. *Cell Cycle* 2007;6(5):620–5. <https://doi.org/10.4161/cc.6.5.3927>. PMID: 17351341.
- [15] Zhou N, Huang Q, Cheng W, et al. p27kip1 haploinsufficiency preserves myocardial function in the early stages of myocardial infarction via Atg5-mediated autophagy flux restoration. *Mol Med Rep* 2019;20(4):3840–8. <https://doi.org/10.3892/mmr.2019.10632>.
- [16] Zhang M, Wang Z, Cheng Q, et al. Circular RNA (circRNA) CDYL induces myocardial regeneration by ceRNA after myocardial infarction. *Med Sci Monit* 2020;26:. <https://doi.org/10.12659/MSM.923188>e923188.
- [17] Zhu Y, Zhao P, Sun L, et al. Overexpression of circRNA SNRK targets miR-103-3p to reduce apoptosis and promote cardiac repair through GSK3 β / β -catenin pathway in rats with myocardial infarction. *Cell Death Discov* 2021;7(1):84. <https://doi.org/10.1038/s41420-021-00467-3>. PMID: 33875647.
- [18] Zheng G, Huang J, Chen W, et al. circUBAP2 exacerbates malignant capabilities of NSCLC by targeting KLF4 through miR-3182 modulation. *Aging* 2021;13(8):11083–95. <https://doi.org/10.18632/aging.202745>. PMID: 33882454.
- [19] Liu B, Tian Y, Chen M, et al. CircUBAP2 promotes MMP9-mediated oncogenic effect via sponging miR-194-3p in hepatocellular carcinoma. *Front Cell Dev Biol* 2021;9:. <https://doi.org/10.3389/fcell.2021.675043>. PMID: 34239873675043.
- [20] Yang W, Sun L, Cao X, et al. Detection of circRNA biomarker for acute myocardial infarction based on system biological analysis of RNA expression. *Front Genet* 2021;12:. <https://doi.org/10.3389/fgene.2021.686116>. PMID: 33995502686116.
- [21] Yang M, Kong DY, Chen JC. Inhibition of miR-148b ameliorates myocardial ischemia/reperfusion injury via regulation of Wnt/ β -catenin signaling pathway. *J Cell Physiol* 2019;234(10):17757–66. <https://doi.org/10.1002/jcp.28401>. PMID: 30820984.
- [22] Chen D, Zhang M. GAS5 regulates diabetic cardiomyopathy via miR-221-3p/p27 axis-associated autophagy. *Mol Med Rep* 2021;23(2):135. <https://doi.org/10.3892/mmr.2020.11774>. PMID: 33313941.
- [23] Zhang Q, Li D, Zhao H, et al. Decitabine attenuates ischemic stroke by reducing astrocytes proliferation in rats. *PLoS One* 2022;17(8):. <https://doi.org/10.1371/journal.pone.0272482>. PMID: 35917376e0272482.